



## Seawater-based mesoporous geopolymer as a sorbent for the removal and recovery of methylene blue from wastewater

M. Padmapriya<sup>a,\*</sup>, S.T. Ramesh<sup>b</sup>, V.M. Biju<sup>a</sup>

<sup>a</sup>Department of Chemistry, National Institute of Technology, Tiruchirapalli 620 015, Tamil Nadu, India, Tel. +91 8946061737; emails: padmapriya2010@gmail.com (M. Padmapriya), vmbiju@nitt.edu (V.M. Biju)

<sup>b</sup>Department of Civil Engineering, National Institute of Technology, Tiruchirapalli 620 015, Tamil Nadu, India; email: stramesh@nitt.edu

Received 29 April 2018; Accepted 12 October 2018

### ABSTRACT

Seawater-based geopolymer (SGP) made from coal fly ash was experimented as a sorbent for the removal of methylene blue using batch sorption process from wastewater. Elemental composition and surface profile of SGP was characterized by different analytical methods such as scanning electron microscopy with energy-dispersive X-ray spectroscopy, Fourier-transform infrared spectroscopy, Brunauer–Emmet–Teller, X-ray fluorescence, and X-ray diffraction analysis. The effect of variables such as solution pH (2–12), the point of zero charge, the contact time, initial dye concentrations (10, 20, and 30 mg/L), SGP dosage (0.01–0.1 g/L), and the temperature (30°C, 40°C and 50°C) was considered to establish optimal experimental conditions. Isotherm experimental result concludes that the Langmuir isotherm suits well than Freundlich isotherm. Results showed that the system forms homogeneous, monolayer with adsorption capacity (59.52 mg/g) by SGP. The kinetic results confirm that the pseudo-second-order sorption well-suited model. The negative values of enthalpy, Gibb's free energy, and entropy reveal that the sorption is exothermic, favorable, and spontaneous with ordered arrangement on the SGP surface. SGP adsorbent was successfully reused up to four cycles and can be considered efficient.

*Keywords:* Seawater-based geopolymer (SGP); Methylene blue (MB); Reusability; Kinetics; Isotherms.

### 1. Introduction

Dye manufacturing and textile finishing industries let off various dyes and pigments untreated in rivers and streams. Organic dyes are extensively used in many activities pertaining to industries such as the coloring process in textile, paper, leather, printing and dyeing sector, food, and cosmetics [1]. It is reported that around 100,000 types of different dyes are manufactured annually with a total quantity of  $7 \times 10^5$  metric tons out of which approximately 100 tons/year are sent out in wastewater [2]. During the dyeing process, the textile industry is the most significant generator of dye effluents. It is estimated that 10%–15% of the dyes do not attach to the fibers and thus remain in the dye bath [3], and 2%–20% are

directly released into aqueous effluents leading to the water bodies [4].

The methylene blue (MB) is a heterocyclic aromatic cationic dye belonging to the thiazine family and carries a positive charge in its molecular structure. MB is commonly used in paper and textile industries, which causes harmful effects to human beings; even though it is not categorized as hazardous, it is acute for living beings [5]. However, all the dyes are harmful pollutants due to their stability in light, heat, and little biodegradation [6–8] or resistant to environmental conditions. Adverse effects include eye irritation, vomiting, diarrhea and jaundice [3], increased heart rate, cyanosis, and tissue necrosis in human beings [9]. Therefore, the removal of

\* Corresponding author.

MB from effluents before its deliverance into the water bodies is prominently essential and needs high priority action.

Various techniques such as adsorption, chemical precipitation, flocculation–coagulation, electrochemical treatment, and ozonation have been adopted for removing water-soluble organic dye-holding wastewater [7,10,11]. Though different methods are available for dye remediation from textile effluents, adsorption is considered the most essential and alternative admirable technique compared with other methods [12,13]. Commercially activated carbon is a very active adsorbent but more expensive compared with other adsorbents [14]. Many researchers have recommended a few more inexpensive adsorbents such as halloysite [10], kaolin [15], pine wood chips [1], red clay [16], and bentonite [17]. Coal fly ash (CFA) is an industrial solid waste liberated by thermal power plants, which increased all over the world, and in India it was about 175 million tons in 2016. This vast quantity creates severe environmental and economic problems [18] and significant challenges in transforming CFA into an efficient and useful material [19–22]. CFA contains a considerable amount of cheap and readily available aluminosilicates with Si and Al source for the manufacturing of zeolites [23] and geopolymers [24,15].

Geopolymers are amorphous semi-crystalline structures [25] formed by a chemical reaction between the Si and Al-enriched materials (aluminosilicates) with a mixture of alkali metal solutions yielding the polymeric structures of Si–O–Al bonds [26,27]. The alkali metal ions (such as Na<sup>+</sup> or K<sup>+</sup>) occupying the voids of the structure to equalize the negative charge of Si and Al [28]. CFA is dissolved briskly into the alkali activator solutions (AAS) resulting in free SiO<sub>4</sub> and AlO<sub>4</sub> tetrahedral structure units by sharing the oxygen atoms and leading to inorganic geopolymer products (–Si–Al– or –Si–Al–Si–).

Aluminosilicates are reformed into the cementitious material (geopolymer) and used as a cost-effective adsorbent for metal [28,29] and dye elimination [30,31] for improved adsorption capacities. In order to synthesize geopolymer, mainly from CFA, some other industrial wastes such as metakaolin [32], blast furnace slag [33], rice husk [34], and bottom ash (BA) [35] can also be used as raw materials. Therefore, geopolymers are seemed to be suitable materials for adsorption. Promising research studies reported that comparing with other adsorbents, the application of geopolymers achieves superiority in the removal of MB from aqueous media due to their porous structure, safe to use, and does not require any pre-treatment for the elimination of pollutants [31].

In this research, the objective is to synthesize seawater-based geopolymer (SGP) from different industrial solid wastes using seawater for the removal of MB and reusability of adsorbent from the aqueous system. There is considerable interest among the researchers on the effect of seawater on geopolymers, as 97% of the earth's water is in the sea. There is not much literature for removal of MB from wastewater using SGP as an adsorbent to the best our knowledge. Hence, this investigation evaluates the adsorption behavior onto SGP adsorbent. Various analytical characterization methods were adopted to explore the physicochemical properties of raw and MB-containing adsorbent. The pH effect on the adsorption of MB by SGP was evaluated from 2 to 12.

Equilibrium isotherms were built at 30°C, 40°C, and 50°C. Adsorption kinetics linear curves were obtained at 10, 20, and 30 mg/L. The thermodynamic studies, desorption, and reutilization were also performed.

## 2. Materials and methods

### 2.1. Raw materials

The CFA F and BA procured from Tuticorin Thermal Power Station, India, was used as waste materials. Ground-granulated blast-furnace slag (GGBS) was obtained from Bellary Steels and Alloys Ltd., Bellary, Karnataka. Laboratory reagent NaOH (97% pure) was used. Sodium silicate was obtained from Kuttuva Silicates Pvt. Ltd., Madurai, Tamil Nadu. The molarity of NaOH solution was kept constant (6 M). The mixture of seawater, NaOH, and sodium silicate was selected as the alkaline liquid (AAS), the source of silica. All the solid particles of the mixture viz. CFA, BA, GGBS, and NaOH pellets ratio were optimized as per the factorial mix design. The cationic dye MB ( $\lambda_{\max} = 664$  nm, molecular weight = 319.86 g/mol, and molecular formula = C<sub>16</sub>H<sub>18</sub>N<sub>3</sub>SCl.3H<sub>2</sub>O) was an adsorbate in this study and was bought from S.D. Fine Chem. Pvt. Ltd., India. The synthetic aqueous solution of MB was prepared by dissolving 1,000 mg/L of distilled water. The working solution was prepared from the stock solution of various concentrations for adsorption experiments.

### 2.2. Synthesis and characterization of SGP

A high alkaline activating solution was made by dissolving solid pellets of sodium hydroxide (6 M) into the sodium silicate solution and dissolved in seawater (36 mL). This mixture is known as AAS. AAS was then allowed to cool and equilibrate for 24 h as it is an exothermic reaction. Similarly, the combination of 20% of CFA with 20% of GGBS and the remaining 60% of BA as filler material was weighed. The chemical composition of sodium silicate solution was Na<sub>2</sub>O = 15.23% and SiO<sub>2</sub> = 35.67% by mass, and the remaining is seawater, and the molar ratio (SiO<sub>2</sub>/Na<sub>2</sub>O) was found to be 2.34. All the reagents were used without purification. SGP adsorbent was prepared by mixing AAS (NaOH, 6.33 g; Na<sub>2</sub>SiO<sub>3</sub>, 72.33 g; and seawater, 36 mL) with the industrial waste (CFA, 100g; GGBS, 100 g; and BA, 303.33 g), made into slurry, and cast as pellets. After 28 d, the hardened paste was crushed well and used for further adsorption studies.

A proximate study was carried out to assess the density, moisture, and loss of ignition (LOI) of SGP adsorbent. The CFA, SGP, and MB-loaded SGP were analyzed by scanning electron microscope (SEM, Vega3, Tescan, Czech Republic) to characterize surface morphology of raw fly ash, coupled with energy-dispersive X-ray (EDX, Bruker nano GmbH, D-12489, Germany), in accelerating voltage 0–30 kV. The samples of CFA, BA, and GGBS were analyzed by X-ray fluorescence (XRF) to find the chemical composition. The major functional groups, present in samples were recorded by Fourier-transform infrared (FTIR) spectra with wavenumber in the range of 4,000–400 cm<sup>-1</sup>. The Brunauer–Emmet–Teller (BET) method is performed to determine the specific surface area. The pore size distributions were obtained from the N<sub>2</sub>

adsorption isotherms by using the Barrett–Joyner–Halenda (BJH) model. X-ray diffraction (XRD) was carried out to study the phases of geopolymer in the range of 2θ–80θ.

### 2.3. Batch adsorption experiments

Batch experiments were performed to assess the influence of contact time and dosage of the SGP adsorbent. The effect of contact time was experimented by different time intervals of SGP (5, 10, 15, 20, 25, 30, 40, 45, 50, 60, 90, 120, 150, and 180 min) with 50 ml solution of 10 mg/L. The effect of dosage was studied by varying the dosage of SGP (from 0.01 to 0.1 g/L) with 10 mg/L of dye concentration for 90 min. The effect of initial dye concentration (10, 20, and 30 mg/L) and initial pH (from 2 to 12) of the solution was studied, and the desired pH of the solution was altered using 0.1 M HCl and 0.1 M NaOH. After the equilibrium time, the samples were taken away at different time periods and centrifuged at 3,600 rpm for 5 min. The supernatant MB solution was analyzed using a UV–visible spectrophotometer (PerkinElmer Lambda 35, Singapore) at 664 nm against a standard calibration curve. The percentage of MB removal efficiency, the quantity of MB uptake at any time ( $q_t$ ), and equilibrium adsorption capacity ( $q_e$ ) can be found by Eqs. (1)–(3), respectively:

$$\text{MB}_{\text{removal}} \% = \frac{C_0 - C_e}{C_0} \times 100 \quad (1)$$

$$q_t = \frac{C_e - C_t}{m} V \quad (2)$$

$$q_e = \frac{C_0 - C_e}{m} V \quad (3)$$

where  $C_0$  and  $C_e$  (mg/L) are primary and equilibrium concentrations of MB in solution, respectively;  $q_t$  (mg/g) is adsorption capacity at specific time;  $C_t$  is remaining MB concentration at time  $t$ ;  $q_e$  (mg/g) is amount of MB adsorbed per unit mass of adsorbent at equilibrium time;  $m$  (g/L) is mass of the adsorbent dosage; and  $V$  (L) is volume of MB solution.

The kinetic experiments were employed with different initial concentrations of dye (10–30 mg/L) agitating at the rate of 150 rpm using orbital shaking incubator for optimized contact period and temperature. The effect of dye concentration can be utilized for the adsorption of equilibrium study. The thermodynamic parameters were calculated from the experimental results of temperature study (30°C, 40°C, and 50°C). All the batch tests were conducted at room temperature (27°C ± 1°C) without pH adjustment.

### 2.4. Adsorption kinetics and isotherm models

Adsorption kinetic method was assessed in this study to evaluate the rate of adsorption. The kinetic adsorption process was analyzed by adopting three familiar kinetic models such as intraparticle diffusion, and pseudo-first-order and pseudo-second-order models. These kinetics studies are widely used in many kinds of literature to understand the process in the sorption of metal and dye [36,37,3]. The pertinence of these kinetics was examined in this study to

calculate the rate of adsorption in SGP. The linear equations of pseudo-first-order and pseudo-second-order equations are listed as Eqs. (4) and (5), respectively [38]:

$$\log(q_e - q_t) = \log q_e - \frac{k_1}{2.303} t \quad (4)$$

$$\frac{t}{q_t} = \frac{1}{k_2 q_e^2} + \frac{1}{q_e} t \quad (5)$$

Where  $q_e$  and  $q_t$  (mg/g) are the adsorption capacities at equilibrium and at time  $t$ , respectively; and  $k_1$  (min<sup>-1</sup>) and  $k_2$  (g/mg min) are rate constants of pseudo-first-order and pseudo-second-order adsorptions, respectively. The plot of pseudo-first-order [ $\log(q_e - q_t)$  vs.  $t$ ] and pseudo-second-order [ $\frac{t}{q_t}$  vs.  $t$ ] was illustrated for all the dye concentration, and the values of  $k_1$ ,  $k_2$ , and  $q_{e,\text{cal}}$  were computed from the slope and intercept, respectively. A plot of  $q_t$  vs.  $t^{1/2}$  was portrayed for all the dye concentration, revealing the boundary layer effect. While the plot passes through the origin, the intraparticle diffusion is the rate-controlling step. Otherwise, some other kinetic mechanism may complicate the adsorption. The intraparticle equation [39] is stated as linear Eq. (6):

$$q_t = k_{\text{id}} t^{1/2} + C \quad (6)$$

The values of  $k_{\text{id}}$  (g/mg min<sup>1/2</sup>) are intraparticle rate constant; and  $C$  is the intercept computed from the slope and intercept.

Adsorption isotherm was explored in this study for understanding the interaction between the adsorbent and adsorbate. The adsorption coverage capacity of MB on SGP was determined using the following isotherm models [21,29].

Langmuir isotherm is vital for this study and widely used for the illustrating dye adsorption at the interfaces of solid/liquid. This isotherm suggests that all adsorption surfaces are identical and limited by mono-coverage adsorption capacity. The linear fashion of Langmuir isotherm model [40] is expressed as follows in Eq. (7):

$$\frac{1}{q_e} = \frac{1}{q_{\text{max}}} \frac{1}{b C_e} + \frac{1}{q_{\text{max}}} \quad (7)$$

where  $b$  is the Langmuir equilibrium constant that indicates heat of adsorption; and  $q_{\text{max}}$  is the maximum mono-

layer adsorption capacity. A plot of  $\frac{1}{q_e}$  vs.  $\frac{1}{C_e}$  was drawn for Langmuir isotherm model for various dye concentrations (10, 20, and 30 mg/L) at 30°C. The values of Langmuir constant ( $b$ ) and adsorption ability ( $q_{\text{max}}$ ) were evaluated from the slope and intercept, respectively. Langmuir isotherm also establishes the viability of adsorption process and stated in terms of Langmuir separation factor ( $R_L$ ) and represented as shown in Eq. (8):

$$R_L = \frac{1}{1 + b C_0} \quad (8)$$

The Freundlich isotherm assumes that the adsorption surfaces show heterogeneity while its surface energies are varying with surface coverage. The linear Freundlich isotherm model [9] is represented by the following Eq. (9):

$$\log q_e = \frac{1}{n} \log C + \log K \quad (9)$$

where  $\log q_e$  is the amount of dye adsorbed per unit mass of adsorbent;  $\log C$  is the equilibrium concentration of adsorbent; and  $K$  is the adsorption capacity constant. A plot of  $\log q_e$  vs.  $\log C$ ,  $n$ , and  $K$  corresponds to intercept, and slope of the linear plot was found for various dye concentration (10, 20, and 30 mg/L) at optimum temperature. Thermodynamic parameters reveal that the change in free energy ( $\Delta G^\circ$ ), entropy ( $\Delta S^\circ$ ), and enthalpy ( $\Delta H^\circ$ ) of adsorption for MB onto SGP was determined using the following Eq. (10) [28]:

$$\ln K_0 = -\frac{\Delta H^\circ}{RT} + \frac{\Delta S^\circ}{R} \quad (10)$$

The plot of  $\ln K_0$  vs.  $\frac{1}{T}$  will give a straight line, and values of  $\frac{\Delta H^\circ}{R}$  and  $\frac{\Delta S^\circ}{R}$  can be evaluated from the intercept and slope, respectively.  $T$  (K) is absolute temperature;  $K_0$  is equilibrium constant; and  $R$  (8.314 J/mol K) is gas constant.  $\Delta H^\circ$  is change in enthalpy;  $\Delta G^\circ$  is standard Gibbs free energy change; and  $\Delta S^\circ$  is change in entropy. The Gibbs free energy change ( $\Delta G^\circ$ ) will be obtained from Eq. (11) [28]:

$$\Delta G^\circ = \Delta H^\circ - T\Delta S^\circ \quad (11)$$

The reusability property of MB-dye bearing SGP was performed with 0.1M of glacial acetic acid at optimal conditions.

### 3. Results and discussion

#### 3.1. Physicochemical properties and characterization of SGP

Proximate testing was executed to assess the moisture, LOI, and density of SGP. About 2 g of adsorbent was kept at 110°C for 60 min and 600°C for 3 h in a hot air oven to estimate the moisture and LOI content, respectively, by Eq. (12):

$$\text{Moisture and LOI content (x)} = \frac{W_2 - W_3}{W_2 - W_1} \times 100 \quad (12)$$

where  $W_1$  is mass of the empty silica crucible;  $W_2$  is weight of the silica crucible plus adsorbent; and  $W_3$  is mass of the silica crucible plus after dried SGP. The density of the SGP was calculated by mass/volume.

From Table 1, it is evident that the SGP after geopolymerization, the moisture and LOI content plays a significant role in the formation of geopolymeric framework by increasing the polymerization. The composition of CFA, BA, and GGBS was determined by XRF. The properties and compositions of significant metal ions in seawater are listed in Table 2.

#### 3.1.1. Surface morphology and BET analysis

SEM was performed to analyze the microstructure of CFA, pre-, and post-adsorbed MB on SGP (Fig. 1). The received CFA (Fig. 1(a)) consists of hollow, glassy, spherical particles known as cenospheres (thin-walled, hollow spheres) confirming that they are from bituminous coal. Although the fly ash particles were mostly the same, variations in shape from angular to round did exist with some crystals of mullite and iron [21].

Duxson et al. [41] investigated geopolymers with Si/Al  $\geq$  1.65; they seemed homogeneous with porosity scattered in small pores mainly when Si/Al is 1.73 as observed from SGP micrograph (Fig. 1(b)). In polymerization, when the concentration of NaOH is more, smaller units of spherical CFA merged and formed as a significant mass of gel [42]. Higher dosage of GGBS in geopolymer paste mixes helps to

Table 2  
Properties of seawater analyzed by Geochemical Laboratory, Trichy

Parameters (mg/L)	Value
Electrical conductivity	60,000
Alkalinity as CaCO <sub>3</sub>	120
Total dissolved solids	36,206
Total Hardness as CaCO <sub>3</sub>	7,600
HCO <sub>3</sub> <sup>-</sup>	146
NO <sub>3</sub> <sup>-</sup>	2
Cl <sup>-</sup>	20,561
Na <sup>+</sup>	10,097
Mg <sup>2+</sup>	1,835
SO <sub>4</sub> <sup>2-</sup>	3,264
Ca <sup>2+</sup>	22
K <sup>+</sup>	352
F <sup>-</sup>	1.22

Table 1  
Physicochemical properties of CFA, BA, and GGBS

Composition of CFA, BA, and GGBS determined by XRF									Physical properties of SGP	
Mass percentage of oxides	SiO <sub>2</sub>	Al <sub>2</sub> O <sub>3</sub>	Fe <sub>2</sub> O <sub>3</sub>	CaO	SO <sub>3</sub>	FeO	MgO	Others	Property	Value
CFA	53.3	29.5	10.7	7.6	1.8	–	–	–	Moisture	4.10%
BA	56.76	21.34	5.98	2.88	0.72	–	–	–	Density	1.34 g/cm <sup>3</sup>
GGBS	35.47	19.36	–	33.25	–	0.8	8.69	3.25	Loss of ignition	8.59%

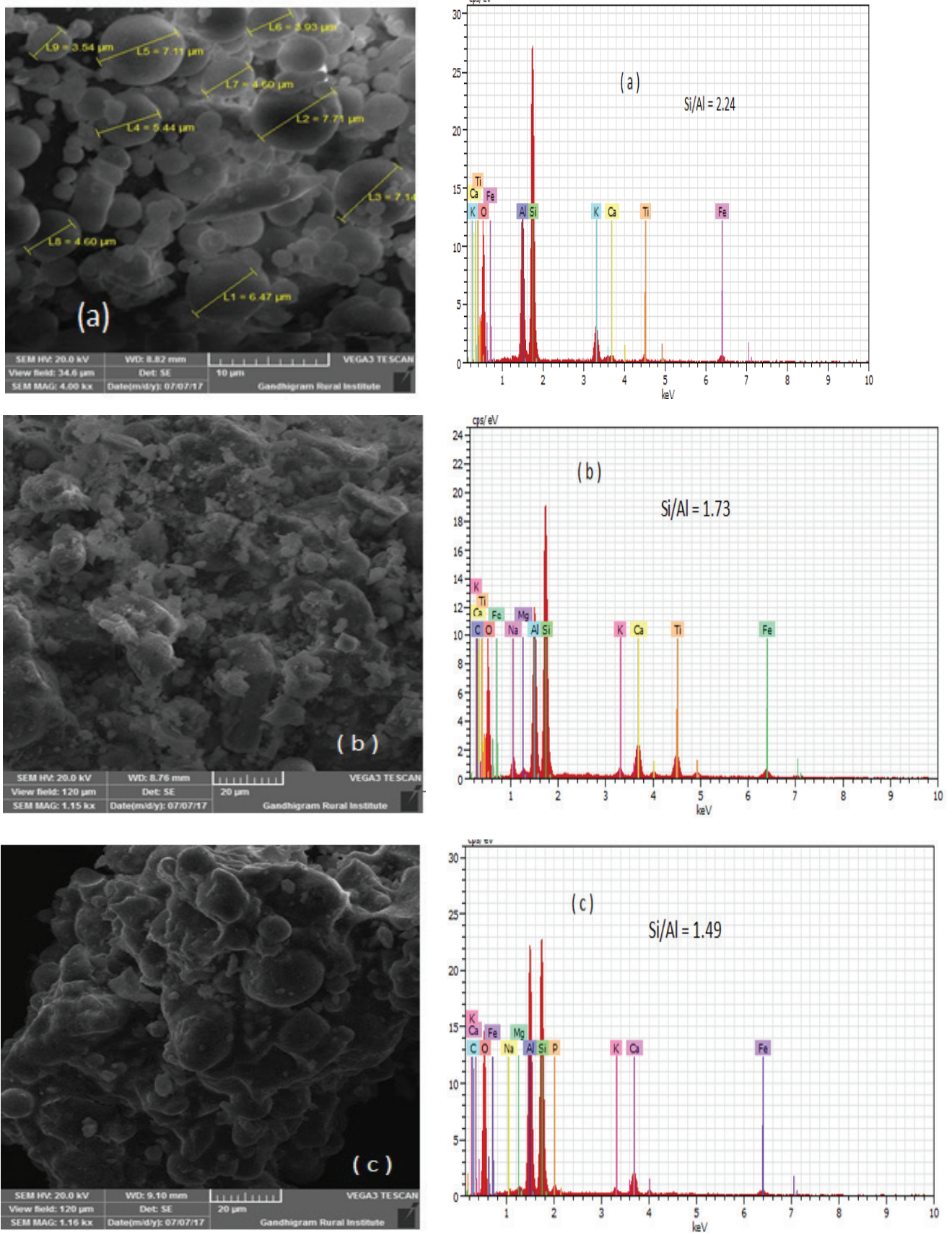


Fig. 1. SEM and EDX images of (a) CFA, (b) SGP, and (c) MB-loaded SGP.

build a denser structure [43] of geopolymer. There was high alkaline attack on the smaller CFA particles, which were trapped inside, and the larger ones were exposed along with some unreacted fly ash present on the SGP before the adsorption of MB. The partially reacted fly ash particles are bonded with geopolymeric gel (Fig. 1(b)). NaOH is distributed over the surface of the adsorbent due to dehydration of seawater.

The chlorides present in seawater (Table 2) in no way harm the structure in alkaline medium. The chloride anions are becoming trapped within the geopolymeric network [44]. The 3D structure of inorganic polymers shows Si and Al atoms as tightly bounded tetrahedral in the geopolymeric network, and the surface of the geopolymer gel is covered with MB dye molecules (Fig. 1(c)). From EDX analysis, Si/Al ratio was found to be 1.49, which was less as compared with SGP before adsorption by the surface active Si and Al elements that interact with MB dye.

The BA particles are much larger than CFA with an irregular structure. BA acts as a filler material during geopolymerization. They do not take part in the chemical reaction. However, the unreacted CFA and BA act as micro-aggregates in linking the paste. Apart from adhered water, the SGP pores tend to absorb water because of its mesoporous structure, which was confirmed by FTIR analysis.

SGP sample is tested for the surface area along with the distribution of pore size using BET analysis and BJH adsorption model [31]. The specific surface area of SGP is found to be 11.85 m<sup>2</sup>/g, and BJH adsorption cumulative pore volume is 0.025 cm<sup>3</sup>/g for SGP. The SGP surface area (11.85 m<sup>2</sup>/g) is relatively high when compared with the phosphoric acid-based geopolymer having surface area 2.28 m<sup>2</sup>/g [31]. The BJH pore volume of SGP is 0.025 cm<sup>3</sup>/g. This high surface area is supplying more surface active sites on the adsorbent, resulting in improved adsorption capacity. The micro, meso, and macro-pore size distribution of SGP is observed in Fig. 2, and its surface topology properties such as specific surface area, pore volume, and size values were tabulated (Table 3).

The type IV isotherm with clearly manifested hysteresis loop H-1 (associated with capillary condensation) by IUPAC indicates the presence of the mesoporous structure with cylindrical pores. The hysteresis loop is type H2 showing that there is a uniform pore diameter distribution.

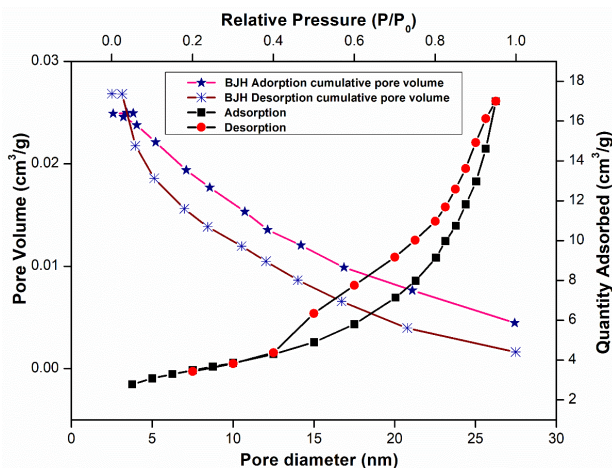


Fig. 2. Surface area and pore analysis of SGP.

The average pore diameter of the adsorbent was 26 nm, suggesting the existence of a mesoporous structure. The more specific surface area is supportive of the adsorbate molecules move toward the adsorbent surface active sites, which could enrich the adsorption efficiency. The total pore volume of SGP at  $P/P_0 = 0.95$  was found as 0.026 cm<sup>3</sup>/g, signifying that SGP adsorbent has a capillary condensation in mesoporous structure and makes it favorable for MB dye to infiltrate into the mesoporous of adsorbent.  $P/P_0 > 0.4$ , which is the direct evidence of the presence of mesopores is represented in Fig. 2.

### 3.1.2. FTIR analysis

The FTIR spectra of CFA, SGP, and MB dye-holding SGP are shown in Fig. 3. The spectra reveal the difference between the CFA and geopolymers [29,45]. The absorption bands exhibited at 3,045, 1,652–3,471, and 1,632–3,444 cm<sup>-1</sup> vibrations for CFA, SGP, and MB loaded on the geopolymer, respectively, corresponds to –OH bending and stretching vibrations due to hydration of seawater [35]. The fly ash peaks at 776 and 907 cm<sup>-1</sup> are assigned to quartz and mullite [45], and noticeable changes were also observed for the SGP and MB loaded on the SGP. The existence of broad peak can be found for SGP at 2,700–3,600 cm<sup>-1</sup> and for MB-loaded SGP at 2,900–3,700 cm<sup>-1</sup>. The peaks get altered indicating the Si–OH

Table 3  
Surface textural properties of SGP

Parameters		SGP
Surface area	BET surface area	11.85 m <sup>2</sup> /g
	Micropore surface area	2.87 m <sup>2</sup> /g
	Mesopore surface area <sup>a</sup>	8.98 m <sup>2</sup> /g
Pore volume	Total pore volume	0.026 cm <sup>3</sup> /g
	Micropore volume	0.001 cm <sup>3</sup> /g
	Mesopore volume <sup>b</sup>	0.025 cm <sup>3</sup> /g
Pore size	Average pore width	8.88 nm

<sup>a</sup>Mesopore surface area = BET specific surface area–micropore surface area.

<sup>b</sup>Mesopore volume = total pore volume–micropore volume.

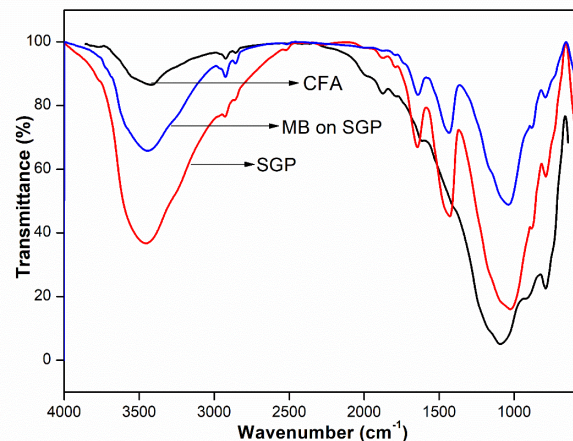


Fig. 3. FTIR analysis of CFA, SGP, and MB-loaded SGP.

(Silonal) groups with  $\text{MB}^+$  ion and formed  $\text{SiO-MB}$  [21]. The band  $1,424$  and  $1,437 \text{ cm}^{-1}$  ascribed in stretching vibrations of  $\text{O-C-O}$  bond in all the samples specifies the presence of sodium hydrogen carbonate [46].

The original CFA bands at  $1,094 \text{ cm}^{-1}$  correspond to asymmetric stretching vibrations of  $\text{Si-O-Si}$  and  $\text{Al-O-Si}$ , and shifting toward the lower wavenumber at  $1,027$  and  $1,033 \text{ cm}^{-1}$  was due to the formation of new geopolymeric reaction [49]. The peaks at  $857$  and  $779 \text{ cm}^{-1}$  for SGP bending vibrations of  $\text{Si-O-Si}$  and  $\text{O-Si-O}$  to the existence of quartz affects the CFA. The peaks at  $857$  and  $785 \text{ cm}^{-1}$  for SGP on MB bending vibrations of  $\text{Si-O-Si}$  and  $\text{O-Si-O}$  specify the occurrence of mullite [47]. FTIR spectra indicate geopolymerization reaction leading to the formation of amorphous aluminosilicates.

### 3.1.3. XRD analysis

XRD analysis [33,43] of CFA and SGP (Fig. 4) samples mainly consists of both amorphous and crystalline phases dominated by hematite ( $\text{Fe}_2\text{O}_3$ ), quartz ( $\text{SiO}_2$ ), magnetite, and mullite. In SGP, a new crystalline silicate compound was found along with amorphous gel when the NaOH concentration is high (6 M). A relatively higher level of geopolymerization takes place in the adsorbent with seawater. The CFA particles readily dissociate in seawater-based AAS enabling in better geopolymerization.

The materialization of aluminosilicate hydrate gel depends on the concentration of alkali (NaOH). Figs. 1(a) and (b) EDX exhibit the association between the Si/Al ratio for CFA and SGP. The ratios of Si:Al was found to be 2.24:1 for CFA and 1.73:1 for SGP. The Si/Al ratio decreased, and discharge of Si and Al occurs due to NaOH concentration. Somna et al. [48] reported that, at low NaOH concentration, the release of Si was higher than the release of Al. Hence, the formation of  $\text{Al-O-Si}$  bond is predominant rather than  $\text{Si-O-Si}$  leading to polymerization of aluminosilicate and silicate in this high alkaline solution. The crystalline phase of SGP disappeared due to advanced geopolymerization with seawater when  $2\theta = 34$  under high alkaline conditions (Fig. 4).

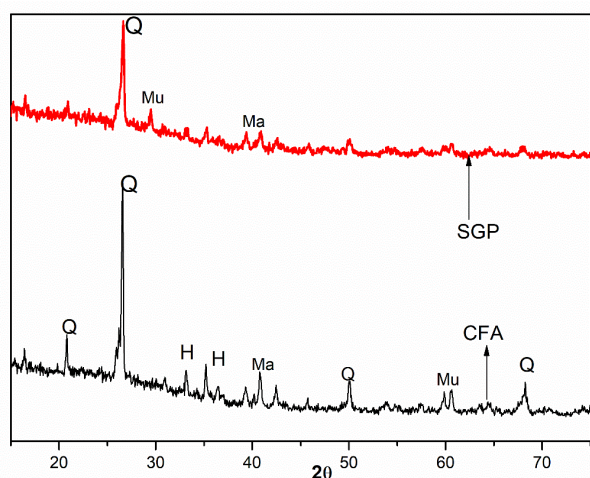


Fig. 4. XRD analysis of CFA and SGP (Q, quartz; H, hematite; Mu, mullite; Ma, magnetite).

## 3.2. Batch experiments

### 3.2.1. Effect of adsorbent dosage

The influence of SGP dosage on the elimination of MB was investigated by varying the quantities of geopolymer dosage from  $0.01$  to  $0.1 \text{ g/L}$  into the flask having  $50 \text{ mL}$  of MB solution ( $10 \text{ mg/L}$ ) at  $30^\circ\text{C}$ . The samples were stirred continuously at  $150 \text{ rpm}$  for  $90 \text{ min}$ . Fig. 5(a) describes the percentage removal and adsorption capacity of MB. The color degradation increases from  $23.51\%$  to  $83.49\%$  as the adsorbent dosage increases because of the existence of active vacant sites on the adsorbent [49]. Further increase in the dosage makes the efficiency almost constant as the surface of the adsorbent becomes saturated. The adsorption capacity reduced from  $235.10$  to  $83.49 \text{ mg/g}$  when the adsorbent dosage increased due to lack of MB in aqueous solution. For an optimum dosage of  $80 \text{ mg/L}$ , the maximum MB removal and adsorption capacity correspond to  $81.35\%$  and  $101.70 \text{ mg/g}$  at  $30^\circ\text{C}$ .

### 3.2.2. Effect of contact time and initial concentration

The performance of interaction time and initial dye concentration for the adsorptive removal of MB from aqueous solution was tested, and results are shown in Fig. 5(b). Dye uptake ability increased from  $13.74\%$  to  $93.03\%$  in  $180 \text{ min}$ . It gradually increases and attains the equilibrium time in  $90 \text{ min}$ , and  $88.05\%$  removal is obtained (Fig. 5(b)). The percentage of MB color elimination decreased with increased initial dye concentration due to the mass transfer resistance

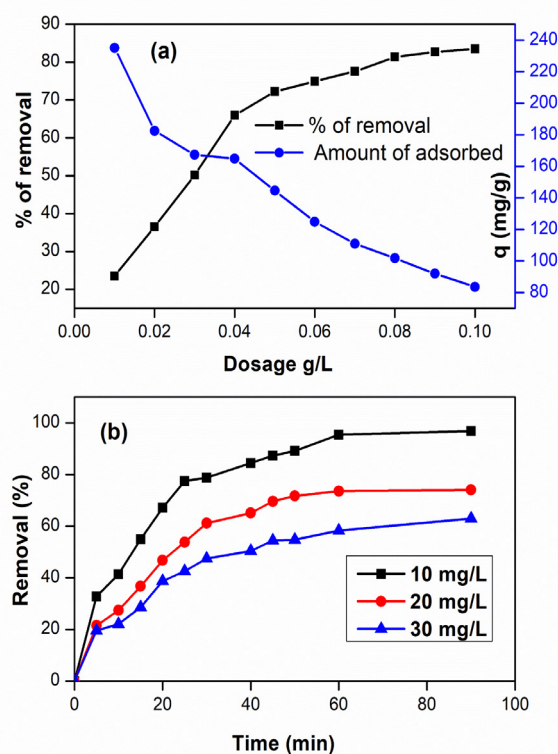


Fig. 5. Effect of (a) dosage and (b) initial dye concentrations on SGP.

of MB in aqueous to the solid phase of the increased SGP (Fig. 5(b)). While the percentage of MB removal capacity was achieved to be 96.80% for 10 mg/L of initial dye concentration, this value was 74.06% and 62.96% for that of 20 and 30 mg/L dye concentration, respectively. At lower dye concentration, the removing capability of SGP was high due to the attraction of MB toward its mesoporous silicon surface with active gel. The elimination of MB was faster at first stages up to 90 min for all initial dye concentration studied. Beyond 90 min, the dye-removing capacity reached equilibrium.

During adsorption, a dynamic equilibrium exists in-between desorption and adsorption of MB after reaching the 90 min of interaction time. During initial adsorption, the MB dye interacted on the boundary layer by mass transfer. Later, the adsorbate slightly diffuses into the boundary layer, enters into the film on SGP, and diffuses into its porous structure. Then they slowly move from boundary layer film on the SGP due to abundant availability of external surfaces. Finally, they diffuse on the porous structure of the SGP. Gautam et al. [50] have proposed a similar explanation using mustard husk for the removal of Alizarin Red S.

### 3.2.3. Effect of pH

The computation of a point of zero charge ( $\text{pH}_{\text{PZC}}$ ) of SGP was achieved based on the solid addition method [51] using 0.01 M  $\text{NaNO}_3$ . The graph of difference in pH ( $\Delta\text{pH} = \text{pH}_i - \text{pH}_f$ ) was plotted against  $\text{pH}_i$ .

By adjusting the solution pH with a strong acidic/basic solution, the adsorption capacity gets affected. The changed pH solution alters the sorption process by influencing the active sites of the adsorbent. Fig. 6 illustrates the outcome of the pH on the SGP by the adsorption of MB. When the pH increased from 2.44 to 4.9, the adsorption capacity reduced. The dye adsorption is reduced when the pH is acidic due to electrostatic repulsion between the positively charged adsorbent and adsorbate ions. When the solution pH value gradually increased from 4.9 to 11.8, the adsorption capacity also increased and attained almost constant. Hence, the maximum adsorption of MB was at pH 11.02, and removal efficiency was 63.54%.

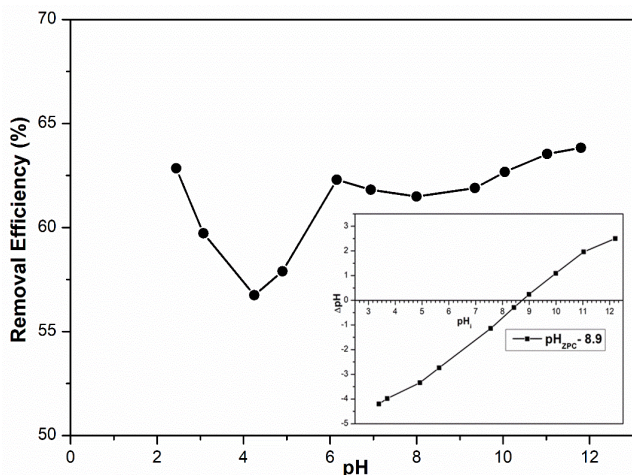


Fig. 6. Effect of pH and zero point of charge (inserted) on SGP.

If the pH approaches the  $\text{pH}_{\text{PZC}}$  of the SGP (8.9, Fig. 6), there is a decrease in the surface charge density and ultimately lowers the electrostatic repulsion between the ions. When excess hydroxyl ions were added, the number of  $\text{H}^+$  ions was decreased while hydroxyl ions enhanced on the site of the adsorbent. The electrostatic interaction between  $\text{MB}^+$  and the negative surface of SGP increased the adsorption affinity when the pH is higher. Theoretically,  $\text{pH} < \text{pH}_{\text{PZC}}$  means the adsorbent surface is positive and favors anionic dye adsorption; and  $\text{pH} > \text{pH}_{\text{PZC}}$  means the surface is negative and favors cationic dye adsorption. However, SGP adsorbent prepared from the high alkaline medium, as a result, the surface consists of more hydroxyl group. Hence, when  $\text{pH} > 8.9$ , there exist more hydroxyl groups and cationic dye adsorption is favorable on the surface. Further study on the dye adsorption characteristics was performed without pH adjustment.

## 4. Kinetic and isotherms study

### 4.1. Modeling of kinetic data

Adsorption kinetics is helpful to design the rate of the interaction between the molecules and the rate-controlling step. The kinetic mechanism namely pseudo-second-order model, pseudo-first-order model, and intraparticle diffusion model were analyzed in understanding the sorption pathway of MB onto SGP. The illustration of these kinetic models is stated in Eqs. (4)–(6). At different dye concentrations (10–30 mg/L) of MB, the pseudo-second-order model was most suited when compared with the pseudo-first-order model. The equilibrium capacity for both models is comparable, and pseudo-second order is close to that of the experimental values  $q_e$  (Figs. 7(a) and (b)). Better regression coefficient ( $R^2$ ) values (Table 4) for pseudo-second order (0.98, 0.95, and 0.95) than for pseudo-first order (0.93, 0.93, and 0.99) suggests its suitability for sorption of MB on geopolymers. The  $k_2$  values diminish with the increase in the initial concentration possibly due to the higher racing for the adsorption sites at a higher concentration compared with lower dye concentration [52]. Therefore, the kinetics model recommends that the MB adsorption onto SGP follow pseudo-second-order mechanism, which is analogous to the research findings of Elkady et al. [53].

The intraparticle diffusion ( $k_{\text{id}}$ ) employed to explore the changes that occurred in the concentration of sorbate onto sorbent with 90 min of shaking time. The kinetic intraparticle diffusion model ( $k_{\text{id}}$ ) for MB sorption onto SGP is calculated using the slope of the plot (Table 4; Fig. 7(c)). It can be seen from Fig. 7(c) that the plot is not passing through the origin confirms that the intraparticle diffusion is not only rate-limiting step other mechanism controls the adsorption.

The  $k_{\text{id}}$  values increase with increasing the initial dye concentrations due to more driving forces. Fig. 7(c) shows three stages of the MB adsorption at different concentration. The first stage represents the external surface adsorption, which is rapid within the first 5 min of shaking time. The second stage is gradual sorption and controlled by intraparticle diffusion rate while the third stage indicates the slow equilibrium stage [54]. The lower  $R^2$  values (0.92, 0.96, and 0.96) than that of the pseudo-second-order model implies that the adsorption process of MB-SGP.

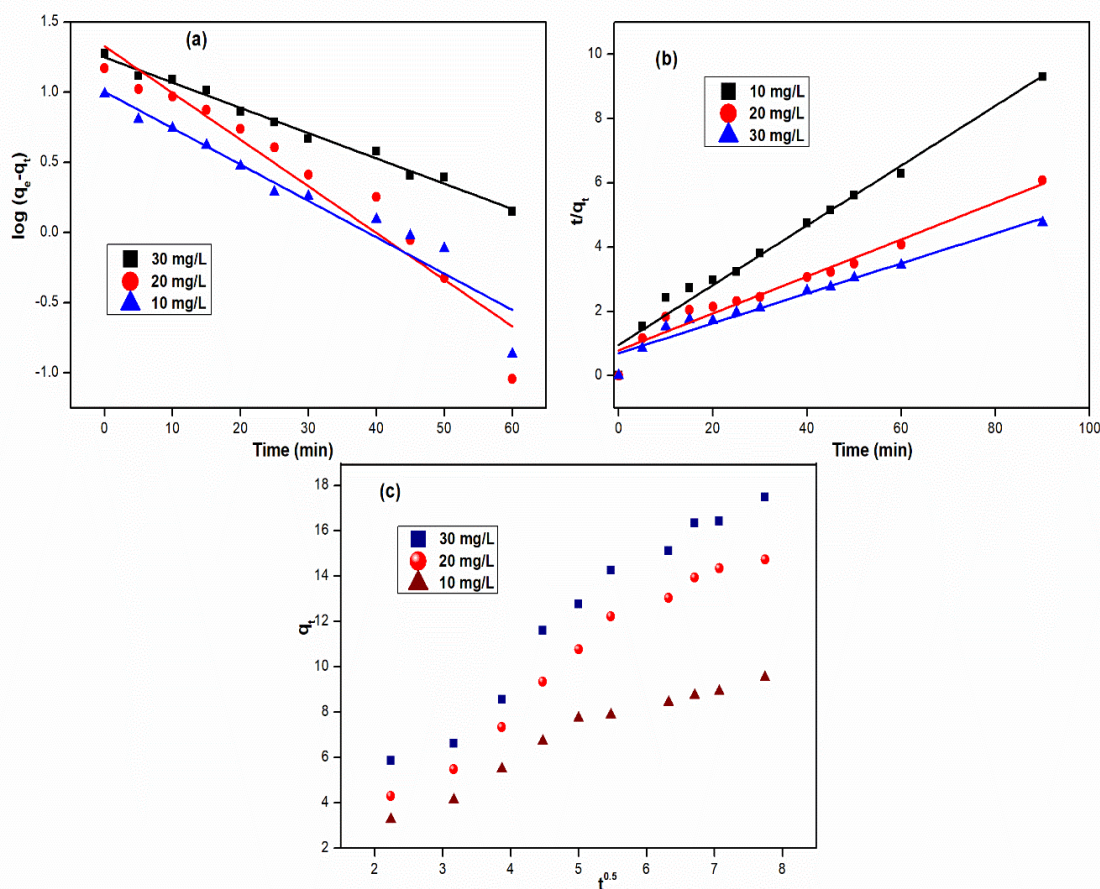


Fig. 7. (a) Pseudo-first-order, (b) pseudo-second-order. and (c) intraparticle diffusion kinetic plots for MB on SGP at different concentrations.

Table 4  
Kinetic parameters for adsorption of MB on SGP for different concentrations at 30°C

MB dye concentrations (mg/L)	Pseudo-first order				Pseudo-second order			Intraparticle diffusion		
	$K_1$ (min <sup>-1</sup> )	$q_{e,exp}$ (mg/g)	$q_{e,cal}$ (mg/g)	$R^2$	$K_2$ (g/mg min)	$q_e$ (mg/g)	$R^2$	$K_{id}$ (mg/g min <sup>1/2</sup> )	Intercept	$R^2$
10	0.06	9.68	10.08	0.93	$9.06 \times 10^{-3}$	10.75	0.98	0.77	3.59	0.92
20	0.08	14.81	21.27	0.93	$4.19 \times 10^{-3}$	17.39	0.95	1.85	1.48	0.96
30	0.04	18.89	17.75	0.99	$3.12 \times 10^{-3}$	21.46	0.95	1.87	3.47	0.96

#### 4.2. Sorption isotherm

In the recent study, Langmuir and Freundlich isotherm models were tested using Eqs. (7)–(9). Fig. 8(a) presents the linear plot that describes the experimental results followed by Langmuir’s isotherm (Table 5). Adsorption coverage capacity ( $q_{max}$ ) and Langmuir constant ( $b$ ) were evaluated and the results are summarized (Table 5). These data suggest that adsorption coverage capacity ( $q_{max}$ , 59.52 mg/g) values confirm the monolayer formation on the SGP sorbent. The monolayer adsorption coverage capacity decreased (59.52, 25.97, and 14.35 mg/g) with increase in temperature (30°C, 40°C, and 50°C) as mobility of MB was hindered. Hence, at lower temperature, there is a higher possibility for the MB

dye being adsorbed on the SGP surface. The dimensionless separation factor ( $R_L$ ) was established using Eq. (8). The  $R_L$  values ( $R_L = 1$  corresponds to linear;  $0 < R_L < 1$  is favorable;  $R_L = 0$  is irreversible; and  $R_L > 1$  is unfavorable) lie less than one indicating that SGP is favorable for MB adsorption under these conditions. The higher regression ( $R^2$ ) values (0.96–0.86) indicated the Langmuir model fitness to the sorption process.

The Freundlich isotherm (Eq. (9)) was adopted when active sites possess heterogeneity on the surface with different energies on the sorbent. Freundlich adsorption capacity ( $K_F$ ) and intensity ( $1/n$ ) were determined from the graph (Fig. 8(b)) to calculate values at a temperature of 30°C, 40°C, and 50°C (Table 5). The lower  $R^2$  values (0.94, 0.94, and 0.83)

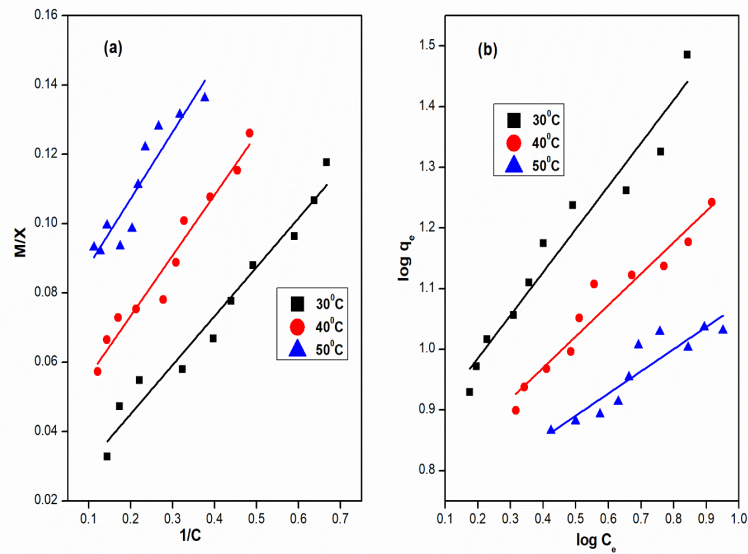


Fig. 8. (a) Langmuir and (b) Freundlich isotherm plots of MB on SGP at different temperatures.

Table 5  
Isotherm constants for the removal of MB on SGP at different temperature

Isotherm models	Temperature (°C)		
	30	40	50
Langmuir			
$q_{\max}$ (mg/g)	59.52	25.97	14.35
$b$ (L/mg)	0.12	0.22	0.36
$R_L$	0.46	0.31	0.22
$R^2$	0.96	0.96	0.86
Freundlich			
$K_F$ (mg/g)	6.97	5.79	5.10
$n$	1.41	1.94	2.73
$R^2$	0.94	0.94	0.83

compared with Langmuir model suggest that Freundlich model does not fit the adsorption of MB on the adsorbent. Freundlich adsorption capacity (Table 5) decreases with increase in temperature signifying at high temperature and has less adsorbent affinity towards MB.

The magnitude of the intensity ( $n$ ) endorses the favorability and capacity of the solid/liquid system. Furthermore, the adsorption intensity  $n > 1$  suggests favorable physical [55] adsorption on mesoporous adsorbent [56]. The highest value of  $n$  (Table 5) suggests weak Van der Waals interactions on adsorption bond [57,58]. The adsorption of MB on the SGP although the values of correlation coefficient obtained by Langmuir model are much better than those obtained for Freundlich plot suggesting that the adsorption of MB is homogeneous and monolayer physical adsorption. Hence, it is validated that the SGP was effective for MB adsorption in an aqueous system (Table 6). Variation in MB adsorption capacity is influenced by the properties of the adsorbent and experimental conditions considered.

Table 6  
Langmuir adsorption capacities of MB with various adsorbents

Adsorbent	$q_{\max}$ (mg/g)	References
Phosphoric acid–MK geopolymer	3.3	[31]
<i>Zea mays</i> cob (ZMC) and <i>Citrus limetta</i> peel (CLP)	ZMC—4.44 and CLP—6.36	[37]
Activated fly ash	14.28	[21]
Biomass FA-geopolymer monolith	15.4	[59]
Forming adsorbents from fly ash	33.96	[22]
Coal fly ash geopolymer	50.7	[60]
Kaolin	52.76	[15]
Seawater-based geopolymer	59.52	Present study

#### 4.3. Thermodynamic parameters

The Gibbs free energy change ( $\Delta G^\circ$ ), entropy change ( $\Delta S^\circ$ ), and enthalpy change ( $\Delta H^\circ$ ) of SGP are obtained from the slope and intercept of van't Hoff plot (Fig. 9) by Eqs. (10) and (11). The negative  $\Delta S^\circ$  value reveals a more ordered arrangement at the solid/solution interfaces while negative  $\Delta G^\circ$  implies a spontaneous and favorable sorption process (Table 7). The negative values of  $\Delta H^\circ$  indicate the exothermic process, which is confirmed by the decreasing adsorption with an increase in temperature. The heat emitted during physical adsorption and the magnitude of the heat of condensation falls into the ranges of 2.1–20.9 kJ/mol [61]. The absolute values of  $\Delta H^\circ$  for SGP is 23.29 kJ/mol indicating that MB adsorption by SGP would be attributed to physisorption. Tunali et al. [55] reported a similar enthalpy change.

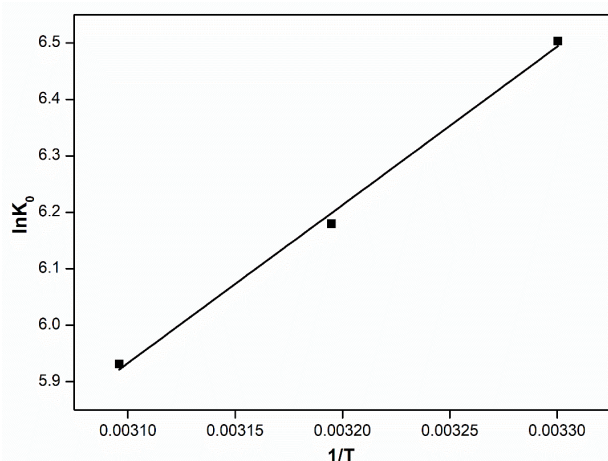


Fig. 9. van't Hoff plot of MB on SGP at different temperatures.

Table 7  
Thermodynamic parameters for adsorption of MB on SGP

Temperature (K)	$\Delta G$ (kJ/mol)	$\Delta H$ (kJ/mol)	$\Delta S$ (J/mol K)
303	-16.38	-23.29	-22.89
313	-16.08		
323	-15.93		

#### 4.4. Reusability of SGP

The sustainable property of the adsorbent can be established by its reusability. In this study, at low pH the adsorption was decreased which indicates the excess  $H^+$  ions to slow down the adsorption mechanism. Therefore, the adsorption/desorption studies performed with 0.1 M of glacial acetic acid up to four cycles confirmed the holding capacity of MB after adsorption from wastewater. The adsorption capacity of MB on SGP decreased from 96.80% to 37.44% (Fig. 10), which indicates that the SGP can be easily reusable after adsorption of MB from aqueous solution.

## 5. Conclusions

SGP is a potential sorbent for the elimination of MB from the wastewater. The specific surface area and pore volume were calculated as 11.85  $m^2/g$  and 0.026  $cm^3/g$ , respectively. The  $pH_{PZC}$  of SGP was found to be 8.9. When the pH is 11.02, the maximum color was removed (63.54%). The optimum SGP dosage was 80 mg/L found with 10–30 mg/L initial dye concentration in 90 min equilibrium time and is more than 80%. The Langmuir isotherm offers homogeneous, monolayer, and adsorption affinity (59.52 mg/g), which is relatively higher at 30°C. Pseudo-second-order mechanism supports more, rather than pseudo-first-order equation and intraparticle diffusion. Thermodynamic studies showed the spontaneous, favorable, and exothermic adsorption of MB by SGP. In addition, the magnitude of the adsorption heat (23.29 kJ/mol) indicates a physisorption process. SGP can be easily recycled four times and used as a cost-effective adsorbent for the removal of MB from wastewater.

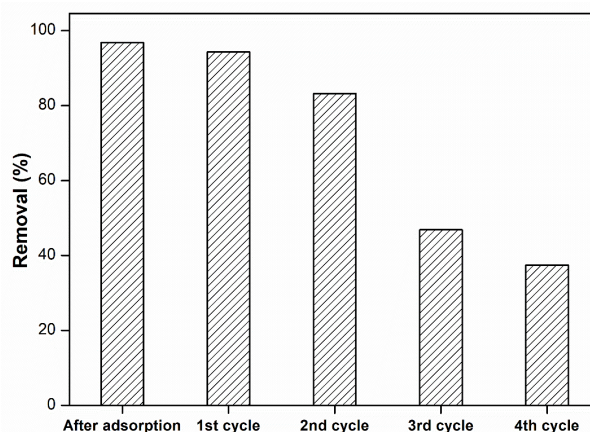


Fig. 10. Reutilization of SGP.

## Acknowledgment

We acknowledge the University Grants Commission, India, for providing permission to pursue Ph.D. under the scheme of Faculty Development Program.

## References

- [1] W. Kong, F. Zhao, H. Guan, Y. Zhao, H. Zhang, B. Zhang, Highly adsorptive mesoporous carbon from biomass using molten-salt route, *J. Mater. Sci.*, 51 (2016) 6793–6800.
- [2] Y.H. Magdy, H. Altaher, Kinetic analysis of the adsorption of dyes from high strength wastewater on cement kiln dust, *J. Environ. Chem. Eng.*, 6 (2018) 834–841.
- [3] N. Mokhtar, E.A. Aziz, A. Aris, W.F.W. Ishak, N.S.M. Ali, Biosorption of azo-dye using marine macro-alga of *Eucheama Spinosum*, *J. Environ. Chem. Eng.*, 5 (2017) 5721–5731.
- [4] M. Bounaas, A. Bouguettoucha, D. Chebli, A. Reffas, I. Harizi, F. Rouabah, A. Amrane, High efficiency of methylene blue removal using a novel low-cost acid treated forest wastes, *Cupressus sempervirens* cones: experimental results and modeling, *Part. Sci. Technol.*, 6351 (2018) 1–10.
- [5] M.T. Yagub, T.K. Sen, S. Afroze, H.M. Ang, Dye and its removal from aqueous solution by adsorption: a review, *Adv. Colloid Interface Sci.*, 209 (2014) 172–184.
- [6] T. Ngulube, J.R. Gumbo, V. Masindi, A. Maity, An update on synthetic dyes adsorption onto clay based minerals: a state-of-art review, *J. Environ. Manage.*, 191 (2017) 35–57.
- [7] G. Liu, Z. Hu, R. Guan, Y. Zhao, H. Zhang, B. Zhang, Efficient removal of methylene blue in aqueous solution by freeze-dried calcium alginate beads, *Korean J. Chem. Eng.*, 33 (2016) 3141–3148.
- [8] Y. Lu, H. Shang, H. Guan, Y. Zhao, H. Zhang, B. Zhang, Enhanced visible-light photocatalytic activity of  $BiVO_4$  microstructures via annealing process, *Superlattices Microstruct.*, 88 (2015) 591–599.
- [9] R.A. Reza, M. Ahmaruzzaman, Comparative study of waste derived adsorbents for sequestering methylene blue from aquatic environment, *J. Environ. Chem. Eng.*, 3 (2015) 395–404.
- [10] P. Luo, B. Zhang, Y. Zhao, J. Wang, H. Zhang, J. Liu, Removal of methylene blue from aqueous solutions by adsorption onto chemically activated halloysite nanotubes, *Korean J. Chem. Eng.*, 28 (2011) 800–807.
- [11] V.K. Gupta, D. Pathania, S. Agarwal, S. Sharma, De-coloration of hazardous dye from water system using chemically modified *Ficus carica* adsorbent, *J. Mol. Liq.*, 174 (2012) 86–94.
- [12] M. Ahmaruzzaman, A review on the utilization of fly ash, *Prog. Energy Combust. Sci.*, 36 (2010) 327–363.
- [13] A.Y.W. Sham, S.M. Notley, Adsorption of organic dyes from aqueous solutions using surfactant exfoliated graphene, *J. Environ. Chem. Eng.*, 6 (2018) 495–504.

- [14] C.F. Carolin, P.S. Kumar, A. Saravanan, G.J. Joshiba, Mu. Naushad, Efficient techniques for the removal of toxic heavy metals from aquatic environment: a review, *J. Environ. Chem. Eng.*, 5 (2017) 2782–2799.
- [15] L. Mouni, L. Belkhir, J.-C. Bollinger, A. Bouzaza, A. Assadi, A. Tirri, F. Dahmoune, K. Madani, H. Remini, Removal of Methylene Blue from aqueous solutions by adsorption on kaolin: kinetic and equilibrium studies, *Appl. Clay Sci.*, 153 (2018) 38–45.
- [16] M.S.U. Rehman, M. Munir, M. Ashfaq, N. Rashid, M.F. Nazar, M. Danish, J.-I. Han, Adsorption of Brilliant Green dye from aqueous solution onto red clay, *Chem. Eng. J.*, 228 (2013) 54–62.
- [17] L.-G. Yan, L.-L. Qin, H.-Q. Yu, S. Li, R.-R. Shan, B. Du, Adsorption of acid dyes from aqueous solution by CTMAB modified bentonite: kinetic and isotherm modeling, *J. Mol. Liq.*, 211 (2015) 1074–1081.
- [18] ENVIS Centre on Fly Ash GOI, 2017. Available at: [http://cbrienvic.nic.in/summaryof\\_fly\\_ash.html](http://cbrienvic.nic.in/summaryof_fly_ash.html)
- [19] H. Cho, D. Oh, K. Kim, A study on removal characteristics of heavy metals from aqueous solution by fly ash, *J. Hazard. Mater.*, 127 (2005) 187–195.
- [20] K. Rastogi, J.N. Sahu, B.C. Meikap, M.N. Biswas, Removal of methylene blue from wastewater using fly ash as an adsorbent by hydrocyclone, *J. Hazard. Mater.*, 158 (2008) 531–540.
- [21] S. Banerjee, G.C. Sharma, M.C. Chattopadhyaya, Y.C. Sharma, Kinetic and equilibrium modeling for the adsorptive removal of methylene blue from aqueous solutions on of activated fly ash (AFSH), *J. Environ. Chem. Eng.*, 2 (2014) 1870–1880.
- [22] Z. Liu, Y. Liu, Structure and properties of forming adsorbents prepared from different particle sizes of coal fly ash, *Chin. J. Chem. Eng.*, 23 (2015) 290–295.
- [23] L.D. Lin, Y. Lin, C.J. Li, D.Y. Wu, H.N. Kong, Synthesis of zeolite/hydrous metal oxide composites from coal fly ash as efficient adsorbents for removal of methylene blue from water, *Int. J. Miner. Process.*, 148 (2016) 32–40.
- [24] L. Li, S. Wang, Z. Zhu, Geopolymeric adsorbents from fly ash for dye removal from aqueous solution, *J. Colloid Interface Sci.*, 300 (2006) 52–59.
- [25] J. Davidovits, Geopolymers and geopolymeric material, *J. Therm. Anal.*, 35 (1989) 429–441.
- [26] R.S. Blissett, N.A. Rowson, A review of the multi-component utilisation of coal fly ash, *Fuel*, 97 (2012) 1–23.
- [27] N.-U. Amin, A multi-directional utilization of different ashes, *RSC Adv.*, 4 (2014) 62769–62788.
- [28] K. Al-Zboon, M.S. Al-Harabsheh, F.B. Hani, Fly ash-based geopolymer for Pb removal from aqueous solution, *J. Hazard. Mater.*, 188 (2011) 414–421.
- [29] M.N. Mužek, S. Svilović, J. Zelić, Kinetic studies of cobalt ion removal from aqueous solutions using fly ash-based geopolymer and zeolite NaX as sorbents, *Sep. Sci. Technol.*, 51 (2016) 2868–2875.
- [30] Y. Zhang, L. Liu, Fly ash-based geopolymer as a novel photocatalyst for degradation of dye from wastewater, *Particuology*, 11 (2013) 353–358.
- [31] M.I. Khan, T.K. Min, A.K. Azizli, S. Sufian, H. Ullah, Z. Man, Effective removal of methylene blue from water using phosphoric acid based geopolymers: synthesis, characterizations and adsorption studies, *RSC Adv.*, 5 (2015) 61410–61420.
- [32] J. Chen, Y. Wang, S. Zhou, X. Lei, Reduction/immobilization processes of hexavalent chromium using metakaolin-based geopolymer, *J. Environ. Chem. Eng.*, 5 (2017) 373–380.
- [33] T. Luukkonen, H. Runtti, M. Niskanen, E.T. Tolonen, M. Sarkkinen, K. Kemppainen, J. Rämö, U. Lassi, Simultaneous removal of Ni(II), As(III), and Sb(III) from spiked mine effluent with metakaolin and blast-furnace-slag geopolymers, *J. Environ. Manage.*, 166 (2016) 579–588.
- [34] S.S. Amritphale, D. Mishra, M. Mudgal, R.K. Chouhan, N. Chandra, A novel green approach for making hybrid inorganic-organic geopolymeric cementitious material utilizing fly ash and rice husk, *J. Environ. Chem. Eng.*, 4 (2016) 3856–3865.
- [35] U.E. ul Haq, S.P. Kunjalukkal, A. Licciulli, Synthesis and characteristics of fly ash and bottom ash based geopolymers—a comparative study, *Ceram. Int.*, 40 (2013) 2965–2971.
- [36] M.S. Al-Harabsheh, K. Al Zboon, L. Al-Makhadmeh, M. Hararah, M. Mahasneh, Fly ash based geopolymer for heavy metal removal: a case study on copper removal, *J. Environ. Chem. Eng.*, 3 (2015) 1669–1677.
- [37] H. Singh, G. Chauhan, A.K. Jain, S.K. Sharma, Adsorptive potential of agricultural wastes for removal of dyes from aqueous solutions, *J. Environ. Chem. Eng.*, 5 (2017) 122–135.
- [38] J. Liu, Y. Wang, Y. Fang, T. Mwamulima, S. Song, C. Peng, Removal of crystal violet and methylene blue from aqueous solutions using the fly ash-based adsorbent material-supported zero-valent iron, *J. Mol. Liq.*, 250 (2018) 468–476.
- [39] S. Kuai, Z. Nan, Formation of sandwich structured  $ZnCe_{0.03}Fe_{1.97}O_4@nSiO_2@SBA-15$  and adsorptive removal of methylene blue from aqueous solution, *Chem. Eng. J.*, 244 (2014) 273–281.
- [40] E.I. El-Shafey, S.N.F. Ali, S. Al-Busafi, H.A.J. Al-Lawati, Preparation and characterization of surface functionalized activated carbons from date palm leaflets and application for methylene blue removal, *J. Environ. Chem. Eng.*, 4 (2016) 2713–2724.
- [41] P. Duxson, J.L. Provis, G.C. Lukey, S.W. Mallicoat, W.M. Kriven, J.S.J. van Deventer, Understanding the relationship between geopolymer composition, microstructure and mechanical properties, *Colloids Surf., A*, 269 (2005) 47–58.
- [42] U. Rattanasak, P. Chindaprasirt, Influence of NaOH solution on the synthesis of fly ash geopolymer, *Miner. Eng.*, 22 (2009) 1073–1078.
- [43] S. Saha, C. Rajasekaran, Enhancement of the properties of fly ash based geopolymer paste by incorporating ground granulated blast furnace slag, *Constr. Build. Mater.*, 146 (2017) 615–620.
- [44] J. Davidovits, Geopolymer, Green Chemistry and Sustainable Development Solutions, *Geopolymer Proceedings*, 2005, p. 10.
- [45] J. Ojima, Determining of crystalline silica in respirable dust samples by infrared spectrophotometry in the presence of interferences, *J. Occup. Health*, 45 (2003) 94–103.
- [46] M.N. Mužek, J. Zelić, D. Jozic, Microstructural characteristics of geopolymers based on alkali-activated fly ash, *Chem. Biochem. Eng. Q.*, 26 (2012) 89–95.
- [47] T. Bakharev, Resistance of geopolymer materials to acid attack, *Cem. Concr. Res.*, 35 (2005) 658–670.
- [48] K. Somna, C. Jaturapitakkul, P. Kajitvichyanukul, P. Chindaprasirt, NaOH-activated ground fly ash geopolymer cured at ambient temperature, *Fuel*, 90 (2011) 2118–2124.
- [49] S. Shakoar, A. Nasar, Groundwater for sustainable development adsorptive treatment of hazardous methylene blue dye from artificially contaminated water using *Cucumis sativus* peel waste as a low-cost adsorbent, *Groundwater Sustainable Dev.*, 5 (2017) 152–159.
- [50] R.K. Gautam, A. Mudhoo, M.C. Chattopadhyaya, Kinetic, equilibrium, thermodynamic studies and spectroscopic analysis of Alizarin Red S removal by mustard husk, *J. Environ. Chem. Eng.*, 1 (2013) 1283–1291.
- [51] N.A. Oladoja, Y.D. Aliu, Snail shell as coagulant aid in the alum precipitation of malachite green from aqua system, *J. Hazard. Mater.*, 164 (2009) 1496–1502.
- [52] M.K. Dahri, M.R.R. Kooh, L.B.L. Lim, Application of *Casuarina equisetifolia* needle for the removal of methylene blue and malachite green dyes from aqueous solution, *Alexandria Eng. J.*, 54 (2015) 1253–1263.
- [53] M.F. Elkady, A.M. Ibrahim, M.M.A. El-Latif, Assessment of the adsorption kinetics, equilibrium and thermodynamic for the potential removal of reactive red dye using eggshell biocomposite beads, *Desalination*, 278 (2011) 412–423.
- [54] K.B. Fontana, E.S. Chaves, J.D.S. Sanchez, E.R.L.R. Watanabe, J.M.T.A. Pietrobelli, G.G. Lenzi, Textile dye removal from aqueous solutions by malt bagasse: isotherm, kinetic and thermodynamic studies, *Ecotoxicol. Environ. Saf.*, 124 (2016) 329–336.
- [55] S. Tunali, A.S. Özcan, A. Özcan, T. Gedikbey, Kinetics and equilibrium studies for the adsorption of Acid Red 57 from aqueous solutions onto calcined-alunite, *J. Hazard. Mater.*, 135 (2006) 141–148.

- [56] P. Patnukao, A. Kongsuwan, P. Pavasant, Batch studies of adsorption of copper and lead on activated carbon from *Eucalyptus camaldulensis* Dehn bark, *J. Environ. Sci.*, 20 (2008) 1028–1034.
- [57] J.-Q. Jiang, C. Cooper, S. Ouki, Comparison of modified montmorillonite adsorbents: Part I: preparation, characterization and phenol adsorption, *Chemosphere*, 47 (2002) 711–716.
- [58] M. Diab, A.Z. El-Sonbati, A.A. El-Bindary, K.S. Mohamed, A.A. Al-Sarawy and M.A. Farid, Removal of hazardous azocoumarin dye from aqueous solutions using activated carbon prepared from rice straw, *Desal. Wat. Treat.*, 57 (2016) 19391–19401.
- [59] R.M. Novais, G. Ascensão, D.M. Tobaldi, M.P. Seabra, J.A. Labrincha, Biomass fly ash geopolymer monoliths for effective methylene blue removal from wastewaters, *J. Cleaner Prod.*, 171 (2018) 783–794.
- [60] Y. Liu, C. Yan, Z. Zhang, Y. Gong, H. Wang, X. Qiu, A facile method for preparation of floatable and permeable fly ash-based geopolymer block, *Mater. Lett.*, 185 (2016) 370–373.
- [61] Y. Liu, Y.-J. Liu, Biosorption isotherms, kinetics and thermodynamics, *Sep. Purif. Technol.*, 61 (2008) 229–242.